Jan P. Scheifers, Kate A. Gibson and Boniface P. T. Fokwa*

Experimental and computational investigations of TilrB: a new ternary boride with $Ti_{1+x}Rh_{2-x+v}Ir_{3-v}B_3$ -type structure

https://doi.org/10.1515/znb-2021-0121 Received August 25, 2021; accepted September 5, 2021; published online September 27, 2021

Abstract: A new ternary phase, TiIrB, was synthesized by arc-melting of the elements and characterized by powder X-ray diffraction. The compound crystallizes in the orthorhombic $\text{Ti}_{1+x}\text{Rh}_{2-x+y}\text{Ir}_{3-y}\text{B}_3$ structure type, space group *Pbam* (no. 55) with the lattice parameters a=8.655(2), b=15.020(2), and c=3.2271(4) Å. Density Functional Theory (DFT) calculations were carried out to understand the electronic structure, including a Bader charge analysis. The charge distribution of TiIrB in the $\text{Ti}_{1+x}\text{Rh}_{2-x+y}\text{Ir}_{3-y}\text{B}_3$ -type phase has been evaluated for the first time, and the results indicate that more electron density is transferred to the boron atoms in the zigzag B_4 units than to isolated boron atoms.

Keywords: Bader charge analysis; borides; density functional theory (DFT); iridium; rhodium; TiIrB; titanium.

Dedicated to: Professor Richard Dronskowski of the Rwth Aachen on the occasion of his 60th birthday.

1 Introduction

We recently reviewed borides with a metal-to-boron ratio (M:B) of 2:1, highlighting their structural variations, relationships, and physical properties [1]. The currently known 130 phases (from binaries to quaternaries) crystallize with 21 structure types. Most of these structures are

Jan P. Scheifers and Kate A. Gibson are co-first authors.

based on B-centered trigonal prisms instead of other modes of coordination, such as those with octahedrally coordinated B atoms. When these prisms share one or more rectangular faces, bonding occurs between neighboring boron atoms. For example, in the MoAlB-type structure infinite zigzag B chains are observed because of shared rectangular faces along the crystallographic c axis [2]. However, many structures with finite boron fragments exist, such as trigonal planar B_4 fragments in the Ti_{1+x} -Os_{2-x}RuB₂ structure [3] and zigzag B_4 fragments in the Ni₃ZnB₂ [4] and Ti_{1+x} Rh_{2-x+y}Ir_{3-y}B₃ [5] structures. Another rare configuration of the B_4 fragment is observed in β-Cr₂IrB₂ [6], where the B_4 fragment is bent, while a second modification, α-Cr₂IrB₂ [6], contains the common zigzag B_4 fragment.

These B₄-based structures have produced some exciting materials including the ferrimagnetic TiCrIr₂B₂ [7] and the superconducting LT-NbOsB [8]. Interestingly, LT-NbOsB remains the only available ternary boride with an orthorhombic $Ti_{1+x}Rh_{2-x+\nu}Ir_{3-\nu}B_3$ -type structure, where Nb occupies the Ti and Rh positions while Os occupies the Ir positions. In addition to the quaternary compound, four other phases were recently presented as part of an exciting series, $Ti_{2-x}M_{1+x-\delta}Ir_{3+\delta}B_3$ (M = Mn-Ni and δ < 0.2) [9], in which a substructure change from trigonal planar B4 units (for M = V - Mn and x = 0.5) to zigzag B_4 units (for M = Mn - Niand x = 0) was observed along the series. Members of the series with early transition metals M = V-Mn crystallize in a hexagonal Ti_{1+x}Os_{2-x}RuB₂-type structure. Consequently, an extrapolation of this series where M = Ti hints at a possible ternary phase, TiIrB, crystallizing with Ti_{1+x}-Os_{2-x}RuB₂-type structure. The only Ti-based ternary phase with this structure containing trigonal planar B₄ units is Ti_{1.6}Os_{2.4}B₂ [10]. As mentioned above, LT-NbOsB is another ternary phase with a M:B of 2:1 that contains B4 units, but crystallizes with the $Ti_{1+x}Rh_{2-x+y}Ir_{3-y}B_3$ -type structure containing a zigzag configuration of the B₄ units instead. We recently also discovered another modification of NbOsB, HT-NbOsB [11], which crystallizes with its own structure type and contains infinite zigzag B chains instead of B₄ units. Herein, we report on the discovery of the anticipated ternary phase "TiIrB", its crystal and electronic structures, as well as its Bader charge analysis.

^{*}Corresponding author: Boniface P. T. Fokwa, Department of Chemistry, University of California, Riverside, CA, 92521, USA, E-mail: bfokwa@ucr.edu. https://orcid.org/0000-0001-9802-7815

Jan P. Scheifers and Kate A. Gibson, Department of Chemistry, University of California, Riverside, CA, 92521, USA. https://orcid.org/0000-0002-9920-7938 (J.P. Scheifers). https://orcid.org/0000-0001-6711-0683 (K.A. Gibson)

2 Results and discussion

2.1 Phase analysis and structure refinement

The TiIrB sample was synthesized by arc-melting of the elements as detailed in the Experimental Section. Phase analysis of the arc-melted product by powder X-ray diffraction (PXRD) indicated four crystalline phases in the sample. Subsequent Rietveld refinement of the PXRD pattern in FullProf [12] generated Figure 1, with results summarized in Table 1. Besides the known TiB₂ (AlB₂ type), TiIr (CuAu type) and TiIr₃ (Cu₃Au type) phases, a new phase could be identified whose lattice parameters and space group (*Pbam*) indicate the $Ti_{1+x}Rh_{2-x+y}Ir_{3-y}B_3$ structure type.

The refined lattice parameters of the new phase are a = 8.655(2), b = 15.020(2), and c = 3.2271(4) Å. These lattice parameters and the unit cell volume are larger than those reported for quaternary phases containing smaller transition metals, M = Mn-Ni [9], and Rhcontaining $Ti_{1+x}Rh_{2-x+\nu}Ir_{3-\nu}B_3$. This is expected since a larger Ti atom replaces the smaller Rh atom. The refined weight fractions (given in Table 1) indicate that the new phase constitutes 27.9(8) wt. % of the sample. To increase the weight fraction of the new phase the amount of iridium in the starting material was increased to a higher ratio, but this change yielded a sample containing less of the targeted phase, even though the formation of

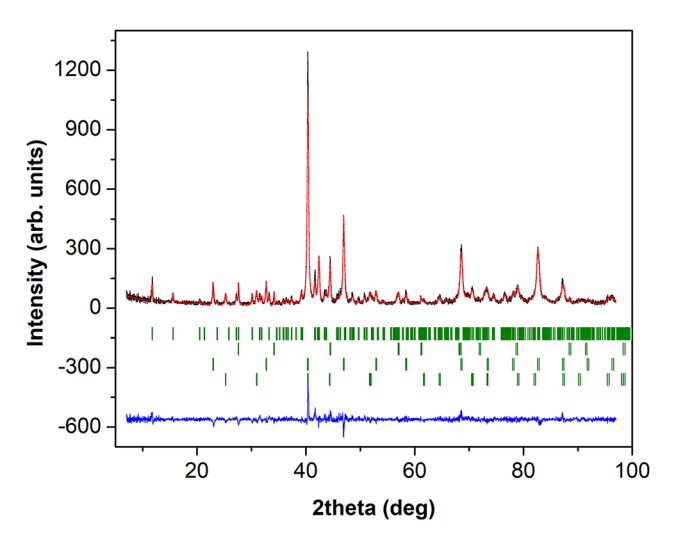


Figure 1: Observed (black) and calculated (red) powder X-ray diffraction pattern of TiIrB; the position of the Bragg reflections (green) for TiIrB (top row), TiB2 (second row), TiIr3 (third row), and of Tilr (bottom row); the difference curve (blue) obtained from Rietveld refinement.

Table 1: Details of the Rietveld refinement for TilrB sample.

Refined composition	Ti _{0.93(1)} Ir _{1.07(1)} B		
Space group, Z	Pbam		
a, Å	8.655(2)		
b, Å	15.020(2)		
c, Å	3.2271(4)		
<i>V</i> , Å ³	419.5(1)		
2θ range, deg	7.02-96.96		
Refinement method	Least-squares		
Profile function	Pseudo-voigt		
R_{Bragg}	9.92		
Fraction, wt. %	27.9(8)		
By-products, fraction, wt. %	TiB ₂ , 14.0(9)		
	Tilr ₃ , 41.6(8)		
	Tilr, 16.5(6)		

TiIr was suppressed. Rietveld refinement was successfully applied to refine the atomic positions and occupational factors for the new phase. For this refinement the asymmetric unit of the $Ti_{1+x}Rh_{2-x+y}Ir_{3-y}B_3$ parent compound was used as the starting model (Figure 2), replacing Rh with Ti and neglecting all mixedoccupancies in the first run. After convergence, mixed occupancies of Ir and Ti were successfully refined on two out of three possible Ti sites (see Table 2), leading to a refined composition of $Ti_{0.93(1)}Ir_{1.07(1)}B$ indicating a phase width with general formula $Ti_{3-x}Ir_{3+x}B_3$. The Ir content mixed on the Ti sites correlates well with the volume of the different coordination polyhedra, with the largest polyhedron exclusively occupied by Ti and the smallest polyhedron containing the highest fraction

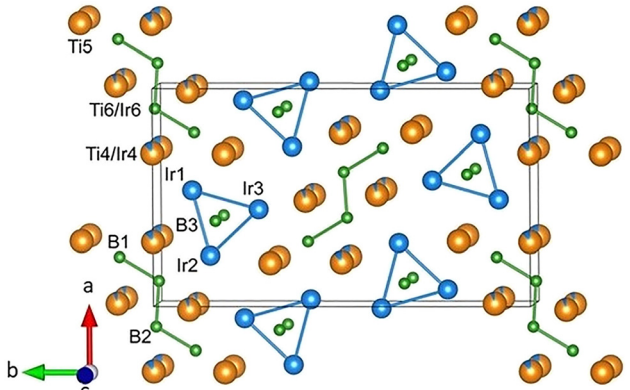


Figure 2: Projected structure of TiIrB ($Ti_{1+x}Rh_{2-x+y}Ir_{3-y}B_3$ type) as obtained from Rietveld refinement.

Table 2: Atomic coordinates from PXRD experiments and DFT calculations and site occupation factors (SOF) for TilrB.

Atom label	Atom label Wyckoff position	X	<i>X</i>	у	<i>y</i>	Z	SOF (PXRD)
		(PXRD) (DFT) ((PXRD)	RD) (DFT)	(PXRD/DFT)		
B3 ^a	4 <i>g</i>	0.107	0.111	0.334	0.333	0	1
B1 ^a	4h	0.214	0.213	0.100	0.099	1/2	1
B2 ^a	4h	0.395	0.396	0.496	0.496	1/2	1
lr1	4h	0.481(1)	0.479	0.094(1)	0.096	1/2	1
lr2	4h	0.281(1)	0.282	0.3586(8)	0.358	1/2	1
Ir3	4h	0.068(1)	0.068	0.2301(7)	0.231	1/2	1
Ti4/Ir4	4 <i>g</i>	0.302(5)	0.299	0.004(2)	0.003	0	0.866(1)/0.134(1)
Ti5	4 <i>g</i>	0.300(6)	0.314	0.204(3)	0.203	0	1
Ti6/Ir6	4 <i>g</i>	0.019(3)	0.017	0.097(3)	0.093	0	0.926(1)/0.074(1)

^aAtomic coordinates are based on geometric considerations and on data of isostructural compounds.

of Ir. The volume of the polyhedra and how it affects the coloring of the different Ti sites has been discussed in more detail for quaternary compounds containing three transition metals [9]. Given that x is very small, we use the ideal composition, TiIrB, for simplification when referring to the new compound. The refined interatomic distances around the B atoms (Table 3) were all within expected ranges as found in borides containing these transition metals, especially those mentioned above that have the same or similar structures [3, 5, 7–11]. The flat B_4 units have bond angles of ca. 117°, which agrees very well with the bond angle in the relaxed computational structure (see electronic structure section below). The B-B interatomic distances are provided without uncertainty as the boron positions have not been refined. However, these coordinates match well with the coordinates of the relaxed structure (Table 2). The chemical bonding analysis performed previously for similar borides containing B₄ fragments has indicated that the boron-based interactions are the strongest bonds [3, 5, 7, 8].

Table 3: Experimental interatomic distances (Å) around the boron atoms in TiIrB obtained from Rietveld refinement.

В3	lr1	2.23(1)
	lr2	2.24(1)
	lr3	2.27(1)
B1	B2	1.83
	Ti4 Ir4	2.29(2)
	lr1	2.31(1)
	Ti6 Ir6	2.34(2)
	Ir3	2.33(1)
	Ti5	2.37(3)
B2	B2	1.82
	B1	1.83
	lr2	2.29(1)
	Ti4 Ir4	2.35(3)
	Ti6 Ir6	2.34(3)
	Ti6 Ir6	2.39(3)

2.2 Electronic structure

The electronic structure was calculated with the Vienna ab Initio Simulation Package (VASP) as detailed in the Experimental Section. The resulting structure, after relaxation, had lattice parameters of a = 8.707, b = 15.094, and c = 3.2412 Åwhich agree with the experimental data. A slight overestimation of all three parameters is observed, as expected from generalized gradient approximation (GGA) calculations. The atomic coordinates after relaxation agree well with the coordinates used for the Rietveld refinement (Table 2).

The total Density of States (DOS) and partial Density of States (pDOS) are illustrated in Figure 3. Boron slightly dominates the low-lying part of the valence band between -9 and -12 eV. Iridium states dominate the DOS below the Fermi energy (E_F) and titanium states dominate above E_F , as expected from their different electronegativities. The Fermi energy is located within a pseudo-gap that extends between -1.5 and 0.5 eV, hinting at an optimized electronic structure and confirming the stability of this phase with an almost ideal composition of TiIrB. However, having a finite DOS at E_F infers metallic character, as expected for this metal-rich boride.

The results of a Bader charge analysis indicate that titanium atoms transfer electron density to Ir and B, as their average valence electron count is 9.81 (instead of 9) and 3.52 (instead of 3), respectively, while that of Ti is 2.67 (instead of 4). Remarkably, the boron atoms in the B_4 zigzag fragments retain higher electron density (charge of -3 per B₄ fragment) compared to the lone boron atoms (charge of -0.025 per lone boron atom). The pDOS of the lone boron atoms and B4 zigzag fragments are compared in Figure 4. The pDOS of B is almost uniform in the range of -1 to -8 eV (see Figure 3), but when divided into two components, the pDOS of the lone B atoms and the pDOS of the B₄ fragments, significant differences become apparent. The pDOS of the B₄ fragments make up most of the boron pDOS

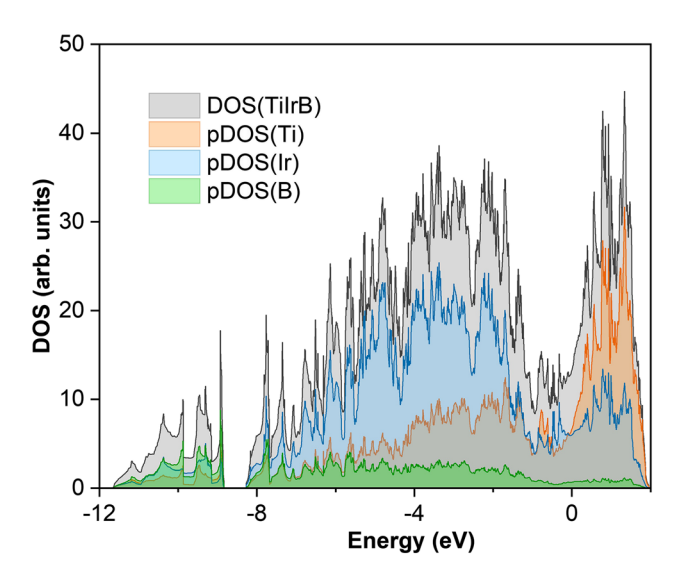


Figure 3: Total and partial density of states (DOS) plots for TilrB.

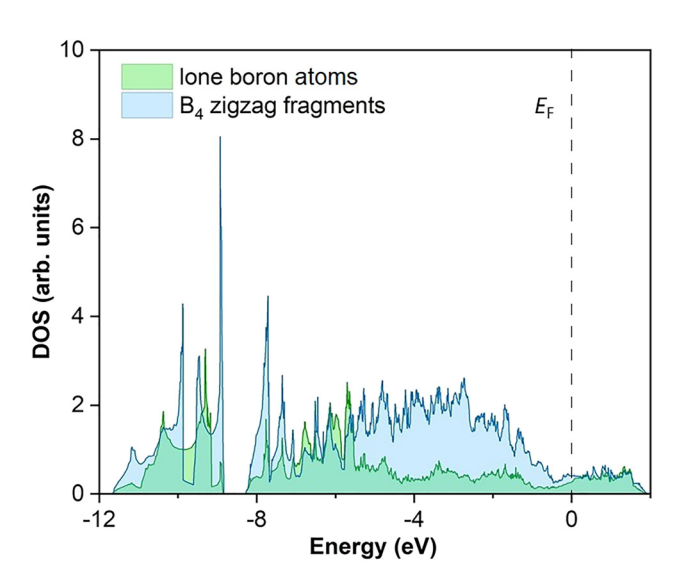


Figure 4: Partial density of states (DOS) plots for the lone boron atoms and the B_A zigzag boron fragments.

in the range of -1 to -5.5 eV compared to that of the lone boron atoms. Thus, it is reasonable to assume that those states are occupied by the additional electrons that have been transferred to the B_4 fragments from Ti. Because of the charge transfer, the atoms at z=1/2 form a negatively charged layer containing Ir atoms and B_4 fragments, and a positively charged layer at z=0 containing Ti and lone B atoms. However, not all valence electrons of Ti have been transferred, so it is plausible to also assume significant metallic bonding between the layers. Furthermore, covalent interactions are expected between the lone boron and the surrounding Ir atoms, as found in similar compounds

[3, 5, 7, 8]. Consequently, a complex mixture of covalent and metallic bonding as well as some level of electron transfer are the major characteristics of this metal-rich boride.

3 Conclusions

We have synthesized the new boride $Ti_{0.94(1)}Ir_{1.06(1)}B$ for the first time and showed that it crystallizes with the orthorhombic $Ti_{1+x}Rh_{2-x+y}Ir_{3-y}B_3$ structure type. The structure was refined based on its powder X-ray diffraction pattern, and the apparent occupational disorder was elucidated. First-principles calculations explored the electronic structure and a Bader charge analysis has shown that electron density is transferred from Ti to both Ir and B. However, the boron atoms building the B_4 fragments inherit more electron density than the isolated B atoms.

4 Experimental section

4.1 Synthesis of TilrB

Ti (99.99%), Ir (99.9%) and B (99% amorphous) were used as purchased from Alfa Aesar, and any air sensitive materials were handled in a glovebox. A starting elemental composition of 1Ti:1Ir:1B was mixed in powder form until a homogenous mixture was obtained before being pressed into a dense pellet. The pellets were then melted in an argon-filled arc furnace. Upon arc-melting, The small metallic bead obtained after arc-melting was powdered and characterized by Powder X-ray Diffraction (PXRD) in a Rigaku MiniFlex 600 instrument with $\text{Cu}K\alpha_1$ radiation (λ = 1.54,059 Å) and a Ge monochromator. The refined experimental values were used to provide the information in Tables 1–3, and Figures 1 and 2.

CSD 2107342 contains the supplementary crystallographic data for this paper. These data can be obtained free of charge from The Cambridge Crystallographic Data Centre via www.ccdc.cam.ac.uk/data_request/cif.

4.2 Computational methods

DFT calculations were used to investigate the electronic structure of the new compound. The TiIrB structural model was prepared in accordance with the ${\rm Ti}_{1+x}{\rm Rh}_{2-x+y}{\rm Ir}_{3-y}{\rm B}_3$ structure type in which the Rh positions were fully occupied by Ti. A model without occupational disorder was used to represent the refined X-ray diffraction data, which showed that less than 12% Ir is mixed on two out of three possible Ti sites. The lattice parameters were relaxed using the projector augmented wave method of Blöchl [13, 14] coded in VASP [15]. All VASP calculations employed the generalized gradient approximation (GGA) with exchange and correlation treated by the Perdew-Burke-Enzerhoff (PBE) functionals [16]. The cutoff energy was 450 eV, and the **k**-point mesh was $19 \times 19 \times 19$. The global break

condition for the electronic SC-loop (E_{diff}) was 1E – 06, and the Fermi level was set to zero. After relaxation, short-circuit (SC) calculations were run. The DOS calculations utilized the CHGCAR file from the SC calculation, with the number of grid points on which the DOS is evaluated (NEDOS) being 2000, making sure to converge the k-points. Bader charge analysis was also performed, ensuring the k-points were converged to ensure an accurate grid for these calculations [17].

Acknowledgment: We thank Dr. Christian Goerens (Umicore) and Dr. Michael Küpers for their contributions during the initial stages of this work.

Author contributions: All the authors have accepted responsibility for the entire content of this submitted manuscript and approved submission.

Research funding: This work was supported by the National Science Foundation Career award to BPTF (no. DMR-1654780).

Conflict of interest statement: The authors declare no conflicts of interest regarding this article.

References

- 1. Iyer A. K., Zhang Y., Scheifers J. P., Fokwa B. P. T. J. Solid State Chem. 2019, 270, 618-635.
- 2. Jeitschko W. Monatsh. Chem. 1966, 97, 1472-1476.

- 3. Fokwa B. P. T., von Appen J., Dronskowski R. Chem. Commun. 2006, 4419-4421; https://doi.org/10.1039/b608903h.
- 4. Malik Z., Grytsiv A., Rogl P., Giester G., Bursik J. J. Solid State Chem. 2013, 198, 150-161.
- 5. Goerens C., Fokwa B. P. T. J. Solid State Chem. 2012, 192, 113-119.
- 6. Kotzott D., Ade M., Hillebrecht H. Solid State Sci. 2008, 10,
- 7. Küpers M., Lutz-Kappelman L., Zhang Y., Miller G. J., Fokwa B. P. T. Inorg. Chem. 2016, 55, 5640-5648.
- 8. Zheng Q., Gumeniuk R., Rosner H., Schnelle W., Prots Y., Burkhardt U., Grin Y., Leithe-Jasper A. J. Phys. Condens. Matter 2015, 27, 415701.
- 9. Scheifers J. P., Küpers M., Zhang Y., Lutz-Kappelman L., Miller G. J., Fokwa B. P. T. Solid State Sci. 2020, 107, 106294.
- 10. Fokwa B. P. T., Dronskowski R. Z. Anorg. Allg. Chem. 2008, 634, 1955-1960.
- 11. Forsythe R., Scheifers J. P., Zhang Y., Fokwa B. P. T. Eur. J. Inorg. Chem. 2018, 2018, 3297-3303.
- 12. Rodríguez-Carvajal R. FULLPROF2000, A program for Rietveld refinement and pattern matching analysis. In Satellite Meeting on Powder Diffraction of the 15th International Congress of the IUCr; Laboratoire Léon Brillouin (CEA-NRS) Gif sur Ivette: Cedex, France, 1990; p. 127, See also: Rodríguez-Carvajal J. Phys. B, 1993, 192, 55-69.
- 13. Blöchl P. E. Phys. Rev. B 1994, 50, 17953-17979.
- 14. Kresse G., Joubert D. Phys. Rev. B 1999, 59, 1758-1775.
- 15. Kresse G., Furthmüller J. Phys. Rev. B 1996, 54, 11169-11186.
- 16. Perdew J. P., Burke K., Ernzerhof M. Phys. Rev. Lett. 1996, 77, 3865-3868.
- 17. Henkelman G., Arnaldsson A., Jónsson H. Comput. Mater. Sci. 2006, 36, 354-360.